Medical Physics
The International Journal of Medical Physics Research and Practice

A planning quality evaluation tool for prostate adaptive IMRT based on machine learning

Xiaofeng Zhu, Yaorong Ge, Taoran Li, Danthai Thongphiew, Fang-Fang Yin, and Q Jackie Wu

Citation: Medical Physics **38**, 719 (2011); doi: 10.1118/1.3539749
View online: http://dx.doi.org/10.1118/1.3539749
View Table of Contents: http://scitation.aip.org/content/aapm/journal/medphys/38/2?ver=pdfcov
Published by the American Association of Physicists in Medicine

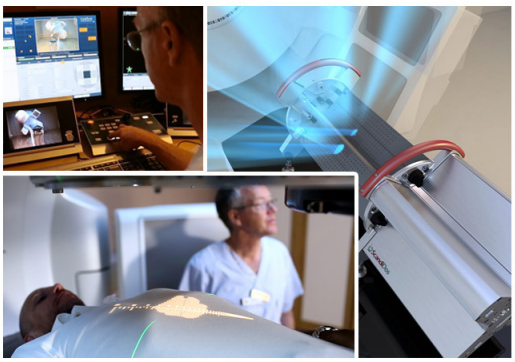

A planning quality evaluation tool for prostate adaptive IMRT based on machine learning

Xiaofeng Zhu[a)]
Department of Radiation Oncology, Duke University Medical Center, Durham, North Carolina 27708

Yaorong Ge
Department of Biomedical Engineering, Wake Forest University Health Sciences, Medical Center Boulevard, Winston-Salem, North Carolina 27106

Taoran Li
Department of Radiation Oncology, Duke University Medical Center, Durham, North Carolina 27708

Danthai Thongphiew
Department of Radiation Oncology, Brody School of Medicine, East Carolina University, Greenville, North Carolina 27834

Fang-Fang Yin and Q Jackie Wu
Department of Radiation Oncology, Duke University Medical Center, Durham, North Carolina 27708

(Received 27 July 2010; revised 15 December 2010; accepted for publication 21 December 2010; published 11 January 2011)

Purpose: To ensure plan quality for adaptive IMRT of the prostate, we developed a quantitative evaluation tool using a machine learning approach. This tool generates dose volume histograms (DVHs) of organs-at-risk (OARs) based on prior plans as a reference, to be compared with the adaptive plan derived from fluence map deformation.
Methods: Under the same configuration using seven-field 15 MV photon beams, DVHs of OARs (bladder and rectum) were estimated based on anatomical information of the patient and a model learned from a database of high quality prior plans. In this study, the anatomical information was characterized by the organ volumes and distance-to-target histogram (DTH). The database consists of 198 high quality prostate plans and was validated with 14 cases outside the training pool. Principal component analysis (PCA) was applied to DVHs and DTHs to quantify their salient features. Then, support vector regression (SVR) was implemented to establish the correlation between the features of the DVH and the anatomical information.
Results: DVH/DTH curves could be characterized sufficiently just using only two or three truncated principal components, thus, patient anatomical information was quantified with reduced numbers of variables. The evaluation of the model using the test data set demonstrated its accuracy ~80% in prediction and effectiveness in improving ART planning quality.
Conclusions: An adaptive IMRT plan quality evaluation tool based on machine learning has been developed, which estimates OAR sparing and provides reference in evaluating ART. © *2011 American Association of Physicists in Medicine*. [DOI: 10.1118/1.3539749]

Key words: plan quality evaluation, adaptive IMRT, machine learning, model training, PCA, SVR

I. INTRODUCTION

Online adaptive radiotherapy (ART) for prostate patients often employs a fast modification of treatment plan to account for interfraction organ motion and deformation. Adaptation approaches vary in plan modification methods but commonly rely on automated fast approximations or optimizations to achieve the desired dose distribution.[1–13] This leads to the risk of degraded plan quality, compared to the original or standard plan that is normally generated without planning time constraints using full-fledged inverse planning and optimization tools from standard IMRT planning algorithms/platforms. Therefore, the ART plans face a critical question as to how well these fast optimized plans compare to the conventional IMRT plans in terms of quality. In our previous research of the feasibility study, we have compared the fast reoptimized plans against the conventionally optimized plans for the same image set. Such head-to-head comparisons are considered as complete comparisons but lacks speed.[14] For clinical implementations, fast quality evaluation of the ART plans is necessary. Moreover, unlike conventional IMRT that uses only a single plan for a treatment course, ART involves multiple treatment planning/reoptimization processes during a treatment course. Therefore, the evaluation of adaptive plans needs to be automatic, consistent, and fast.

After fast approximation, an ART plan achieves high dose coverage at the planning target volume (PTV). In addition, it can often easily meet either the institutional or the Radiation Therapy Oncology Group (RTOG) sparing goals for organs at risk (OARs) in which the constraints are relatively conser-

vative since they are applied to a general population. Therefore, using the DVH indices from these templates does not necessarily ensure that the ART is of as good quality as that of the conventional plan for a specific daily anatomy.

Further, as volume and shape of the OARs and PTV change, the DVH indices and parameters also vary even though the plan quality remains the same. Therefore, this project aims to evaluate the plan quality taking the volume and shape variation into account. An objective estimation of optimal dose volume histograms (DVHs) for OARs based on patient-specific anatomical information provides a direct evaluation of ART plan quality. The optimal DVH for OAR is modeled from prior conventional IMRT plans and serves as the baseline/reference DVH for ART plan evaluation. Therefore, when the ART plan DVH is compared to the reference DVH, the ART plan quality is evaluated against the conventional IMRT technology.

Although the DVH has been adopted in dose evaluation and optimization in radiotherapy for a long time,[15,16] studies on DVH estimation techniques are just starting. Using the fact that dose distribution in radiotherapy is closely constrained by the patient anatomical geometry,[17,18] a method for comparing treatment plans was previously reported using overlap volume histogram (OVH) to infer the likely dose volume levels.[19] This method was implemented by comparing the relative anatomical spatial configurations between patients. However, it could not account for the conditions when those OVH curves entangle. An empirical approach was introduced to estimate OAR dose volume level as a function of input dose volume constraints for all involved OARs, using a minimum knowledge base to model the Pareto surface of IMRT plans.[20] Such an approach might take too long time to be effective for application in online ART. Moreover, none of the existing methods provide estimation of the entire DVH curve.

We present a quantitative evaluation tool for prostate ART based on machine learning, which estimates a baseline DVH for OAR using knowledge learned from prior plans. The estimation model is trained with a supervised approach using the DVHs and anatomical information from 198 high quality plans generated by experienced planners following the institutional planning conventions. The anatomical information consists of the PTV volume, the OAR volumes, and the voxel's distance to the PTV surface, where the distance is roughly inversely correlated with its dose. Principle component analysis (PCA) is used to characterize salient features of DVH and the patient anatomical information and support vector regression (SVR) is used to model their correlation. The accuracy of the estimation and the quality of this evaluation tool are evaluated with 14 additional prostate IMRT plans outside the training pool.

II. METHODS AND MATERIALS

II.A. Patient data

The database and evaluation data set consists of 212 IMRT plans retrospectively selected from 18 prostate cancer patients. Each patient has one computed tomography (CT) scan and ten cone-beam CT (CBCT) scans. The CBCT data were obtained from the first five days (d1–d5) during the first week and the following five weeks (w2–w6). The training data set consists of 198 plans with 11 plans (1 CT +10 CBCT) for each patient.

Those plans were generated using the same procedures and shared the same beam setup. Using the Varian Eclipse treatment planning system (Varian Medical Systems, Palo Alto, CA), contours of the clinical target volume (CTV) (including prostate and seminal vesicles), bladder and rectum were drawn by attending physicians. The PTV corresponded to the CTV plus a 5 mm uniform margin. For prostate cases, the PTV typically features large and random interfractional motions and deformations due to filling in the neighboring rectum and bladder.[21] These deformations, which were also expressed by their organ volume variances, provide a robustness test for the proposed system. All the plans share the same configuration of seven-field 15 MV photon beams, with the gantry angles at 180°, 130°, 70°, 20°, 340°, 290°, and 230°, representing one posterior, two posterior-oblique and four anterior-oblique fields, respectively.

The institutional planning criteria and processes for prostate IMRT treatments were applied. For the PTV, the prescription dose (R_x=78 Gy) should cover at least 95% of the PTV volume, and the maximum dose D_{max} must not exceed 107% Rx. The dosimetric constraints were 70, 62, and 39 Gy to <20%, 30%, and 50% of the bladder volumes and 70, 56, and 39 Gy to <20%, 30%, and 50% of the rectum volumes, respectively. To further spare the OARs, the trial-and-error process was used by experienced planners to iteratively adjust the OAR constraints and to reach a final plan that ensures the OAR dose as low as achievable for each individual plan. All these plans are considered as expert plans (As seen later, 1 or 2 of the plans actually can be further improved on OAR sparing).

II.B. Characteristics of IMRT plans: DVH vs. DTH and volumes

The OAR dose was studied in relation to its anatomical information that is characterized by its volume and distance from PTV. Intuitively, IMRT plans aim for fast dose falloff outside the PTV volume, and, in general, such dose fall-off tends to correlate with the distance from the surface of PTV. For instance, Fig. 1(a) illustrates the fast dose fall-off of an OAR (rectum) from the prostate PTV. The cumulative DVH of the rectum are plotted in Fig. 1(b). Figure 1(c) illustrates the distance-to-target histogram (DTH) which provides a summarized characterization of organ shape relative to PTV. DTH is the fractional volume of the OAR within certain distance from the PTV surface. For voxels inside the PTV, the distance is negative, indicating intrusion/overlap. In this study, the DTHs of the OARs, together with volumes of the PTV and the OARs, constituted the patient-specific anatomical information, which was the input to the DVH estimation model; the output was the DVH curve of each OAR.

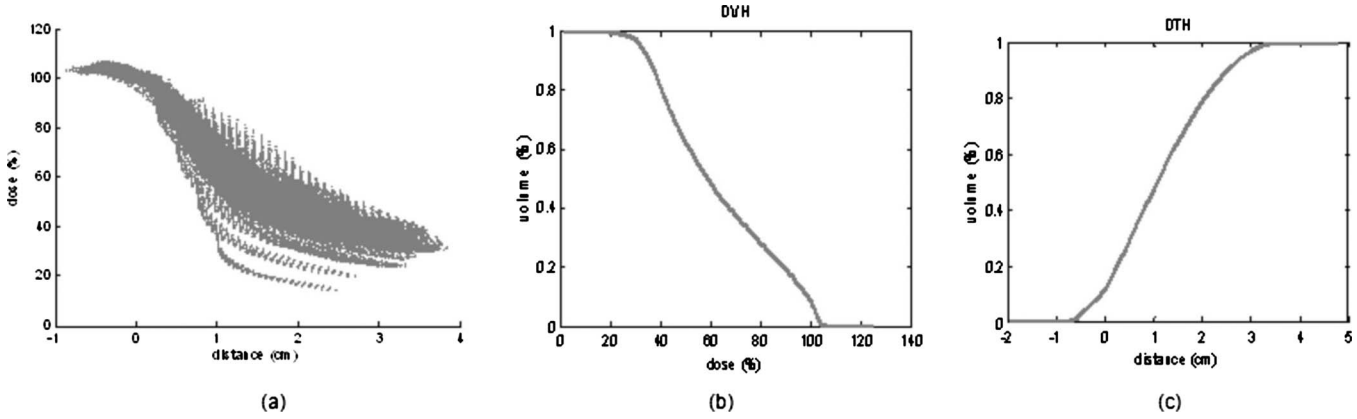

FIG. 1. The relationship between the dose and the distance-to-target for voxels of a patient rectum. (a) shows a scatter plot of the dose at each individual voxel. vs. its distance-to-target; (b) presents the cumulative DVH of the rectum; (c) plots the cumulative DTH of the rectum.

II.C. PCA of DVH and DTH curves

PCA was applied to characterize the DVH and DTH curves with greatly reduced dimensions. PCA is an effective tool widely used for feature selection, which identifies patterns hidden in high dimensions.[22] In this work, each cumulative DVH or DTH was sampled by 50 points and thus was represented by a feature point (or vector) in a 50 dimensional feature space. A total of 198 feature points form the feature space for each OAR (DVH or DTH). The basic idea of PCA is to determine if these feature points are colinear in some dimensions so that they can be represented by a smaller number of dimensions. For example, if all the feature points lie in an oblique 2D plane in this 50D vector with nonzero values in the first two dimensions and zeroes in all the remaining dimensions. In PCA terms, the two nonzero values in the first two dimensions represent the component scores of the principal components of this feature set, and hereafter the component score is denoted as PCS that is a scalar in this paper. In real feature space with noise, it is often sufficient to identify the lower dimensional space that covers (or explains) a large percentage of feature points. For example, in the new coordinate system in the previous example, if the feature points do not lie exact on the 2D plane, but they vary only slightly in the third dimension, then we can still use the first two principal components to faithfully represent these feature points by basically projecting the feature points onto the 2D space formed by the first two dimensions.

To determine the principal components of each set of 198 curves represented as 198 feature points in 50 dimensions, we first translated the original coordinate system so its origin is located at the geometric center of the 198 feature points (call it the shifted coordinate system). Then, we normalized the feature points so the values in each dimension had a mean of 0 and a standard deviation of 1. Finally, we formed a covariance matrix (50×50) of the 198 points in this new coordinate system and performed a singular value decomposition of this covariance matrix which produced 50 eigenvectors and 50 corresponding eigenvalues. According to the PCA theory, the 50 eigenvectors form a new coordinate system (call it the PC coordinate system; basically a rotation of the shifted coordinate system) that identifies the principal components with the corresponding eigenvalues signifying the amount of variations in that component (or dimension). In this new PC coordinate system, the origin represents the center (or average) of the 198 feature points, which basically represents an average of the 198 curves and each dimension conceptually adds a certain amount variation to this average curve. Thus, by choosing a small set of principle components with the largest eigenvalues, we can represent most significant variations of the DVHs or DTHs with a small number of dimensions and thus achieve the goal of feature selection.

Note that we can easily determine the corresponding curve from given values of the selected PCS (two for the bladder and three for the rectum). Conceptually, we first form a 50D vector in the PC coordinate system with given values in the PC dimensions and zeros in all non-PC dimensions. Then we transform this vector from the PC coordinate system back to the original feature space by performing an inverse transformation of the coordinate systems. The resulting feature vector contains the 50 sample points of the curve (DVH or DTH) that corresponds to the given PCS.

II.D. SVR and model training

SVR corresponds to the regression version of support vector machine (SVM). SVM, as a supervised learning method used for data classification,[23,24] is implemented by constructing a set of hyperplanes to separate data of different classes. For complicated problems that are not linearly separable, SVM introduces the kernel function that projects the data into a higher-dimensional space where the projected data become linearly separable. Mathematically, it is modeled as a convex quadratic optimization problem where the error is minimized by maximizing the distance from the hyperplanes. However, SVM is limited to classification problems that have discrete target variables. For regression problems that have continuous target variables, SVR is implemented by introducing a tube of width ε, instead of hyperplanes as in classification, and the problem becomes that of finding a

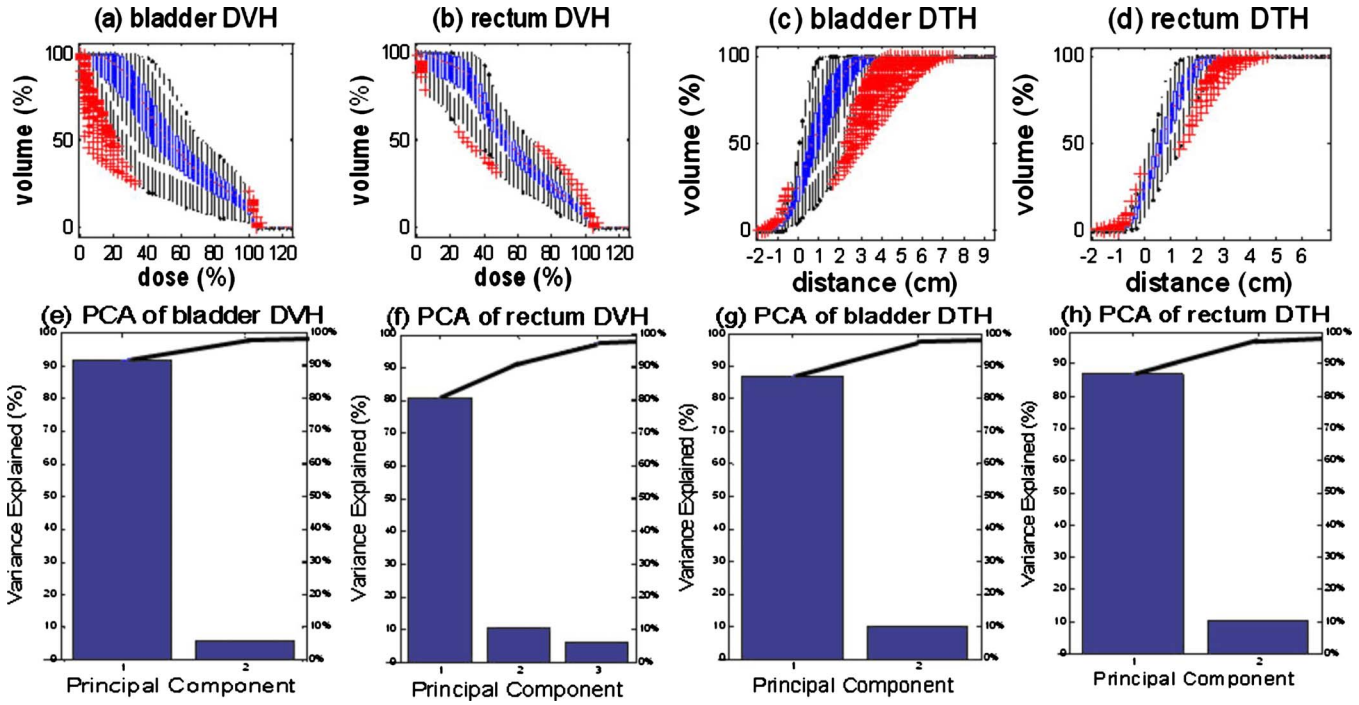

FIG. 2. Results of PCA applied to the training database. (a)–(d) show the statistical dispersion of the DVH/DTH for the bladder/rectum from 198 plans using the box-and-whisker plot: box (central 50%), vertical line (lower and upper 25%), and plus (outliers). (e)–(h) present with the Scree plot the truncated principle component scores (PCS) that account for 90% variance.

function that has at most ε deviation from the actually obtained targets for all the training data, and at the same time is as flat as possible.[25–27]

The goal of training is to establish a functional correlation or mapping between the patient anatomical information (input) and the DVHs of the OARs (output). An *ad hoc* multivariable nonlinear regression (MVNLR) was first introduced as a "quick and dirty" approach to probe the structure of the data set and the correlation among these variables. The MVNLR was implemented by manually adding new fitting terms to minimize the fitting error, which might increase the risk of overfitting. To avoid overfitting, SVR is implemented by minimizing an upper bound on the fitting error tolerance.[28] This was achieved by employing an ε-insensitive loss function where penalty was applied in the SVR objective function only if the fitting error exceeds the tolerance defined by ε.

II.E. Model validation

For patient cases outside the training pool, the DVH for each OAR was estimated using the trained model. First, the new anatomic information was collected including the volumes of the OARs and PTV, as well as the OAR DTHs. Second, the truncated PCSs of the DTH were calculated by multiplying the standardized DTH with the transformation matrix (50×50) that was derived during the learning phase. Third, the truncated PCSs of the DVH were calculated using the trained regression functions. Then, the calculated DVH PCSs were multiplied by the inverse of the aforementioned transformation matrix (50×50), and finally, the estimated DVHs of the OARs were reconstructed after adding onto the mean DVH curve of the training database.

In this study, we visually compared the predicted bands of the DVHs with the "true" DVHs generated by expert planners. If the true DVH falls within the predicted band for a specific plan, then the prediction is considered correct. This is obviously simplistic. Quantitative criteria that account for the importance of dose ranges will be studied in future projects.

III. RESULTS

By applying PCA, the number of variables used to characterize DVH and DTH were reduced from 50 to 2 for bladder or 3 for rectum. In Figs. 2(a)–2(d), statistical dispersions of the DVHs and DTHs for the bladders and rectums are shown with box-and-whisker plots: box (central 50%), vertical line (lower and upper 25%), and plus (outliers), respectively. In the bottom row of the Fig. 2, the percentage of variance represented by individual PC is plotted in descending order as bars, and the cumulative total is represented by lines, only the first 90% of the cumulative distribution is displayed. To cover $>$90% variance, Figs. 2(e), 2(g), and 2(h) show that the first two PCSs are needed for the bladder DVH, the bladder DTH, and the rectum DTH. Figure 2(f) indicates the first three PCSs are needed for the rectum DVH.

The reconstruction of the DVH curve from its truncated PCS is illustrated in Fig. 3. The solid and dash lines in Fig. 3 (left) are the resulting curves if we take the first PCS and the

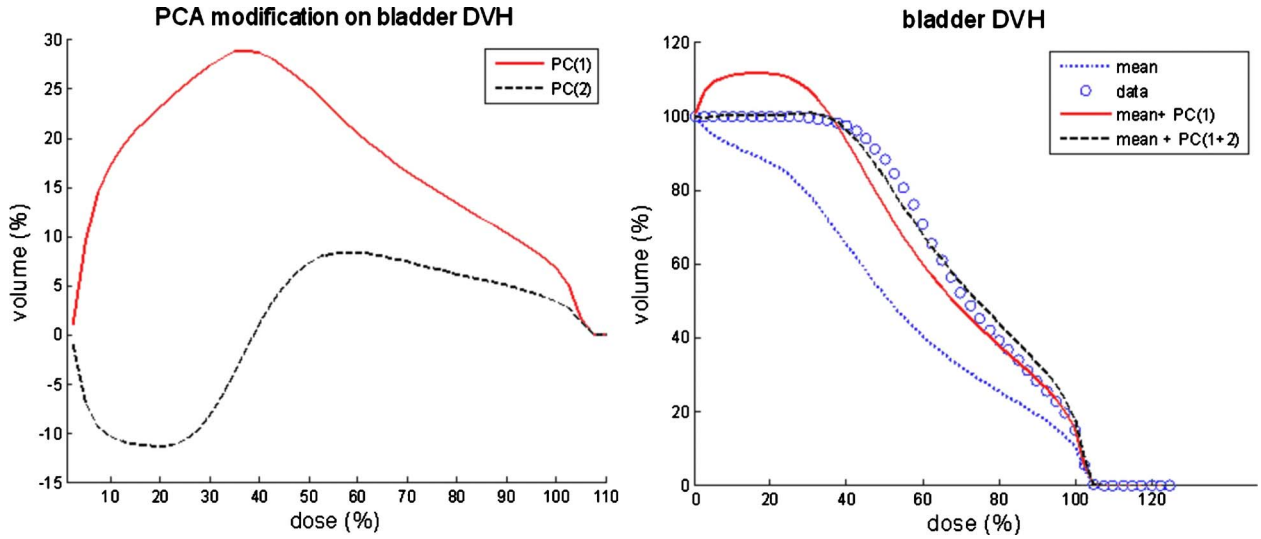

FIG. 3. Reconstruction of the bladder DVH curve using truncated PCS. The left figure shows contribution from the first two PCS. The right illustrates the reconstruction of the DVH curve compared with the original data.

second PCS of the bladder DVH of one patient and transform them back to the shifted coordinate system. In Fig. 3 (right), the dotted line represents the mean bladder DVH curve of the 198 plans and the solid line is the curve of the first PCS transformed from the shifted coordinate system back to the original feature space, i.e., adding the solid line of Fig. 3 (left) to the dotted line of Fig. 3 (right). The dash line of Fig. 3 (right) is the curve of the first two PCSs transformed back to the original feature space. This can be visualized as adding both lines of Fig. 3 (left) to the dotted line of Fig. 3 (right). The circled curve in Fig. 3 (right) is the actual DVH curve from the original plan, which agrees well with the reconstructed curve.

The truncated two or three PCSs, together with organ volumes, composed the variables of the mapping function for model training. For simplicity, we denote the truncated PCS of rectum DVH as: $Y_{\text{DVH\_rect\_1}}$, $Y_{\text{DVH\_rect\_2}}$, $Y_{\text{DVH\_rect\_3}}$, and the rectum DTH as $X_{\text{DTH\_rect\_1}}$, $X_{\text{DTH\_rect\_2}}$. For the bladder, the PCS are $Y_{\text{DVH\_blad\_1}}$, $Y_{\text{DVH\_blad\_2}}$ and $X_{\text{DTH\_blad\_1}}$, $X_{\text{DTH\_blad\_2}}$. The volumes of the PTV, rectum, and bladder were denoted as X_{ptv}, $X_{\text{v\_rect}}$, and $X_{\text{V\_blad}}$, respectively. Thus, the input vector for the mapping function was $\vec{x}$ (X_{ptv}, $X_{\text{v\_rect}}$, $X_{\text{v\_blad}}$, $X_{\text{DTH\_rect\_1}}$, $X_{\text{DTH\_rect\_2}}$, $X_{\text{DTH\_blad\_1}}$, $X_{\text{DTH\_blad\_2}}$), and the outputs were $Y_{\text{DVH\_rect\_1}}$, $Y_{\text{DVH\_rect\_2}}$, $Y_{\text{DVH\_rect\_3}}$, $Y_{\text{DVH\_blad\_1}}$, and $Y_{\text{DVH\_blad\_2}}$. For instance, the first PCS of the rectum DVH was modeled by eight input variables: $Y_{\text{DVH\_rect\_1}} = F_{\text{rect\_1}}(X_{\text{ptv}}, X_{\text{v\_rect}}, X_{\text{v\_blad}}, X_{\text{DTH\_rect\_1}}, X_{\text{DTH\_rect\_2}}, X_{\text{DTH\_blad\_1}}, X_{\text{DTH\_blad\_2}})$.

The correlation between the variables of the DVH and the variables of the patient anatomical information was modeled by MVNLR and SVR, separately. The high dimensionality and complexity of the mapping function, indicated by the fitting equation for MVNLR, was addressed in the SVR kernel function using a Gaussian radial basis function. The high dimensionality and complexity is indicated by the number and form of the fitting terms. As an example of the rectum DVH,

$$
\begin{aligned}
Y_{\text{DVH\_rect\_1}} = {} & a_1 X_{\text{DTH\_rect\_1}} + a_2 X_{\text{DTH\_rect\_2}} + a_3 X_{\text{DTH\_rect\_3}} \\
& + a_4 X_{\text{DTH\_rect\_1}} X_{\text{DTH\_rect\_2}} \\
& + a_5 X_{\text{DTH\_rect\_1}} X_{\text{DTH\_rect\_3}} \\
& + a_6 X_{\text{DTH\_rect\_2}} X_{\text{OVH\_rect\_3}} + a_7 X_{\text{DTH\_rect\_1}}{}^2 \\
& + a_8 X_{\text{DTH\_rect\_1}}{}^3 + a_9 X_{\text{DTH\_rect\_2}}{}^2 \\
& + a_{10} X_{\text{DTH\_rect\_2}}{}^3 + a_{11} X_{\text{DTH\_rect\_1}}{}^2 X_{\text{DTH\_rect\_2}} \\
& + a_{12} X_{\text{DTH\_rect\_1}} X_{\text{o\_rect\_2}}{}^2 \\
& + a_{13} X_{\text{DTH\_rect\_1}} X_{\text{v\_ptv}} + a_{14} X_{\text{DTH\_rect\_2}} X_{\text{ptv}} \\
& + a_{15} X_{\text{DTH\_blad\_1}} + a_{16} X_{\text{v\_ptv}} + a_{17} X_{\text{v\_blad}} \\
& + a_{18} X_{\text{v\_rect}}.
\end{aligned}
$$

The tolerance boundary around the SVR solutions was empirically set to $\varepsilon = 0.2$, which approximates the average fitting error of MVNLR, to accommodate the information loss due to PCS' truncation, uncertainty due to small data set, and noise introduced by plans of nonperfect quality. Figure 4

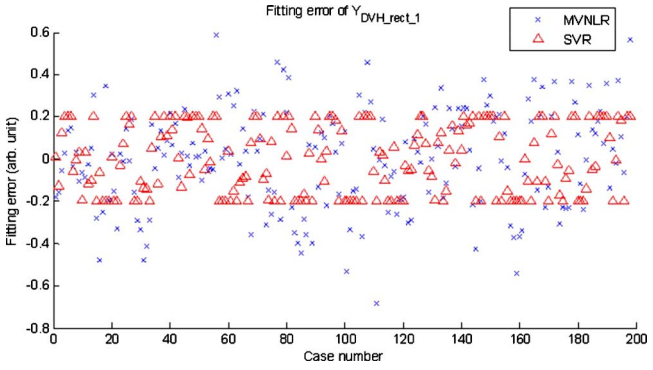

FIG. 4. Comparison of fitting errors using MVNLR and SVR. The fitting error in SVR is managed by the tolerance tube: $\varepsilon = \pm 0.2$, which is chosen empirically to approximate the average fitting error using MVNLR

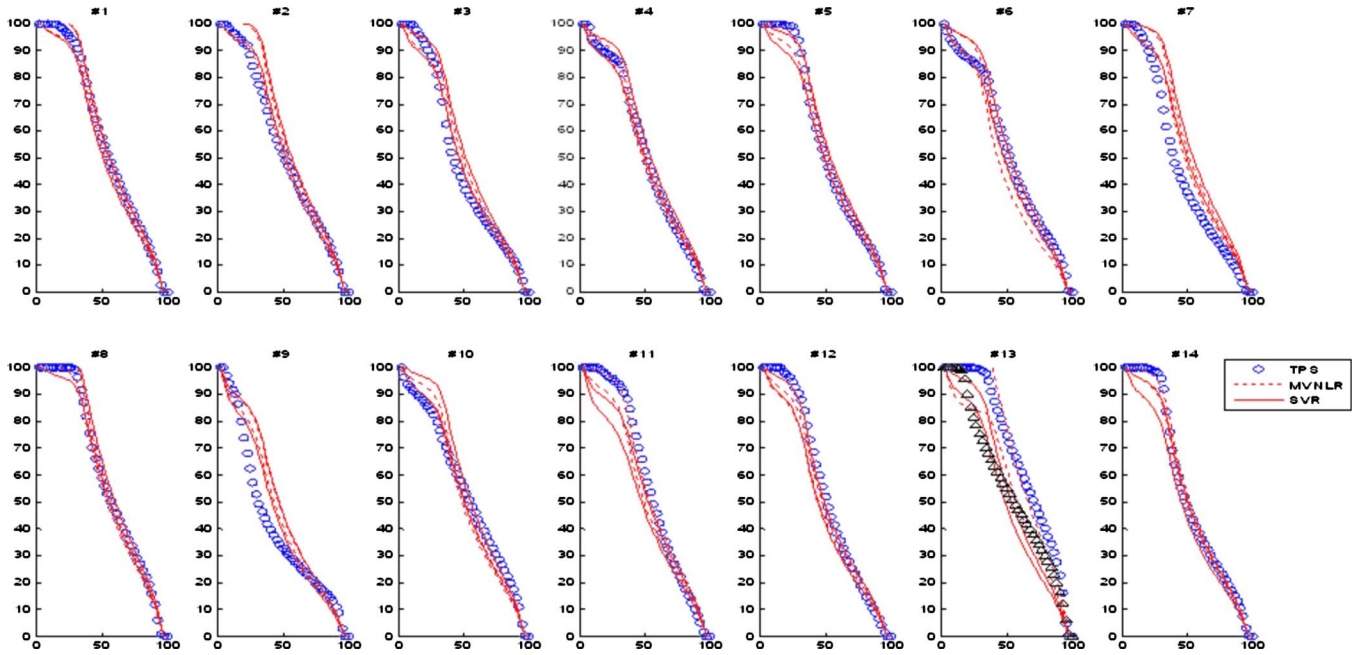

FIG. 5. Model evaluation on rectum using 14 cases outside the training pool. For 11 out of 14 plans, the DVHs generated by the treatment planning system (TPS) are within the prediction bands. The "triangle" shows the result after replanning for case #13.

illustrates the fitting result for the rectum DVH: the fitting errors using MVNLR are shown with "x," and using SVR with "triangle." Overall, 57% of the plans using MVNLR have larger fitting errors than using SVR. All SVR fitting errors lie within the specified tolerance of ± 0.2, whereas 43% of the MVNLR fitting errors are out of the tolerance tube. In this preliminary study, SVR features a manageable control for fitting risk with the selection of ε.

The accuracy of the estimation model was evaluated with 14 prostate patient cases outside the training pool. Figures 5 and 6 show the estimated DVHs for the rectum and bladder of the 14 cases, respectively. The circles show the actual DVH curves generated by expert planners using eclipse treatment planning system (TPS). Using MVNLR, the 95% confidence band of the estimated DVH curves are plotted with dashed lines. The tolerance boundaries $\pm\varepsilon$ are used to recon-

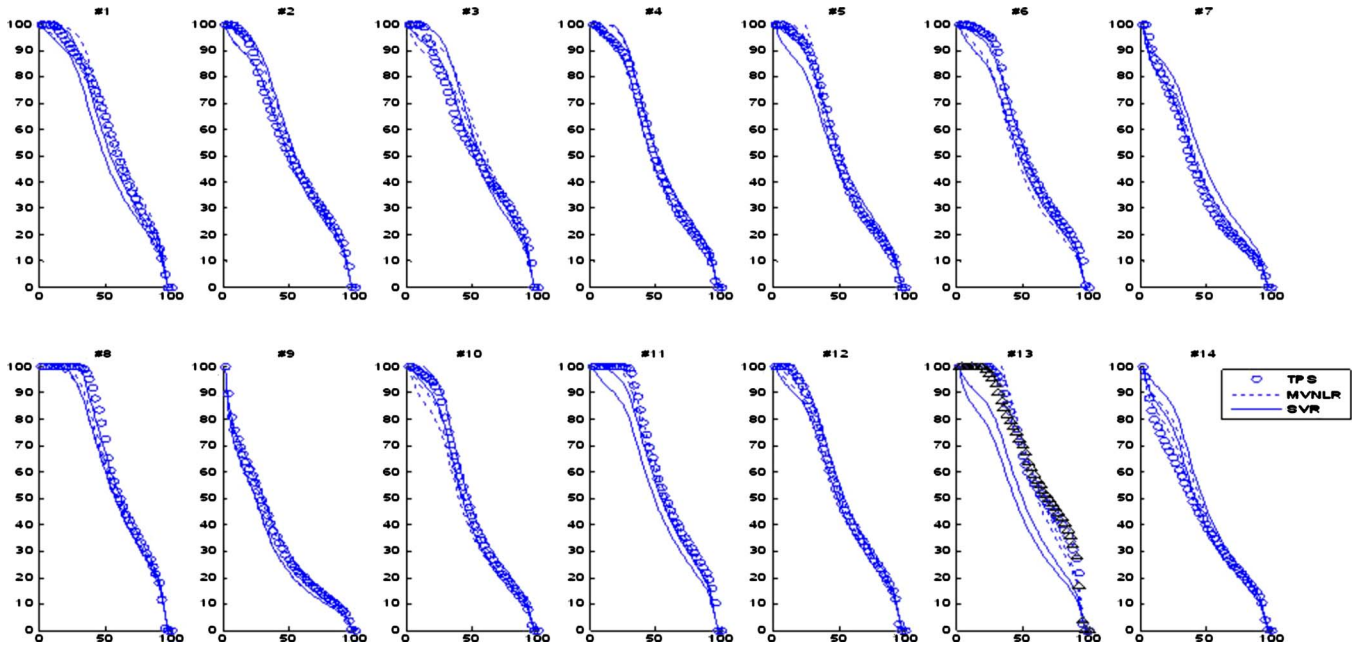

FIG. 6. Model evaluation on bladder using 14 cases outside the training pool. Except for case #13, the DVHs generated by the treatment planning system (TPS) agree with the prediction. The triangle shows the result after replanning for case #13.

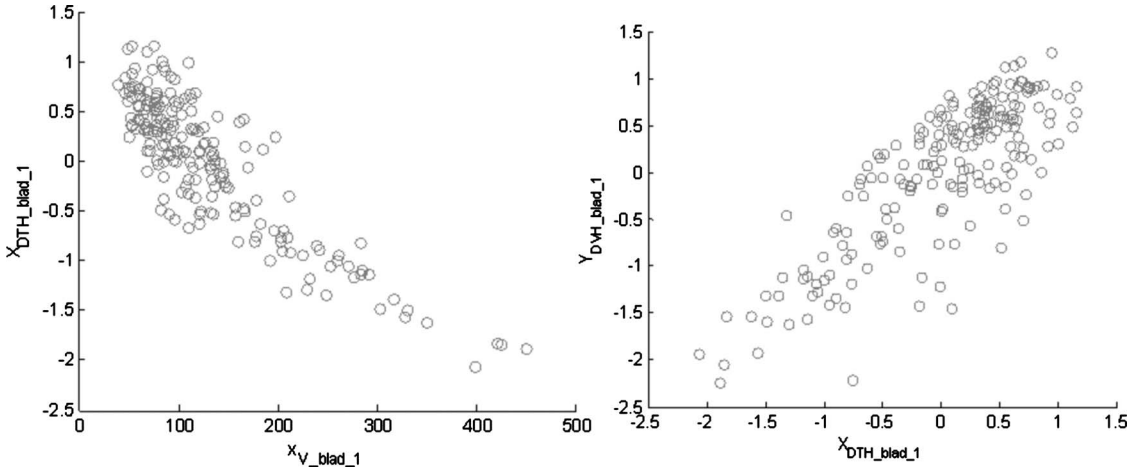

FIG. 7. The correlations among the bladder volume, its first DTH PCS, and its first DVH PCS. The left figure clearly indicates that an increase in bladder volume will inversely increase $X_{\mathrm{DTH\_blad\_1}}$, the mean distance variance. The right indicated the trend between $X_{\mathrm{DTH\_blad\_1}}$ and the mean dose variance $X_{\mathrm{DVH\_blad\_1}}$.

struct the estimation bands for SVR, which are plotted with solid lines. Except for cases #7, 9, and 13, the estimations are successful for 11 out of 14 test plans, i.e., the DVHs created by TPS fall within the bands estimated by either MVNLR or SVR. If a planned DVH shows better sparing in OARs than both estimation bands, e.g., in case #7, it would be added to the training pool in the future study, and as more quality plans accumulate in the training data set, thus, the estimated DVH would improve in the trend of better OAR sparing. For case #13, the evaluation gives warning that the planned DVH has less sparing than the estimations. A subsequent examination revealed the inconsistency of the rectum contouring, i.e., rectum was contoured following a different convention than what was used by plans in the training database, which also explained the big discrepancy between the two estimation bands. After recontouring and replanning, better sparing of the rectum was achieved and the updated DVH is plotted with triangles in Figs. 5 and 6.

IV. DISCUSSION

PCA is straightforward in reducing the number of dimensions, however, it forfeits simple or easy explanations of the PCS.[22] Further study is needed to interpret the clinical/physical meanings of the PCA variables used in the model. As shown in Fig. 3 (left), the first PC for DVH/DTH stands for unidirectional but nonuniform deviations from the mean DVH. The modification from the second PC can be divided into two sections (0%–38% and 38%–100% on the dose axis) with opposite directional and nonuniform deviations. The third PC will apply three sectional modifications, and the same logic applies to the forth and higher modes. From the analysis of 3D-CRT, Sohn *et al.*[29] attributed the first PC to the mean dose variance, which is closely related to the unidirectional deviations in this study. Nevertheless, their correlation in 3D-CRT between the second PC and the organ volume within the two- and four-field overlap region is difficult to be compared directly in our study because the counterpart does not exist in IMRT as the fluence map of IMRT is much more complex than 3D-CRT.

The correlation studies for the PCS confirm the correlations among the dose, distance and organ volumes as mentioned in Introduction. In Fig. 7, a proportional relationship between $Y_{\mathrm{DVH\_blad\_1}}$ and $X_{\mathrm{DTH\_blad\_1}}$ indicates that the mean dose variance (related to the unidirectional deviation) increases as the mean distance variance to the PTV surface decreases, such a correlation could explain the evaluation criteria applied in the quality control tool by Wu *et al.*,[19] which they used the single OVH parameter to characterize this main feature. Similar correlation can also be found among $Y_{\mathrm{DVH\_blad\_1}}$, $X_{\mathrm{DTH\_blad\_1}}$, and $X_{\mathrm{V\_blad}}$, indicating the important role of the bladder volume in affecting both DVH and DTH.

Both regression models, MVNLR and SVR, presented similar results in the DVH estimations in this study which consists of a relatively small data size. As the data size increases, the advantage of SVR in managing overfit will emerge. However, powerful in model generalization, SVR also has its limit in interpreting clinical or physical meaning of its model that includes the abstract hyperplanes. Contrary to SVR, the relationship between clinical and physical meaning terms as depicted in Fig. 7 may be analyzed in MVNLR in a straightforward way. Both regression models will benefit from a larger database in future study.

It should be noted that this study primarily concentrated on the application to online ART where one patient was treated with several plans sharing the same beam configurations. Therefore, factors that also affect plan quality, such as beam energy, number of beams, and the beam orientations, are not considered in the current evaluation model as these factors remain the same for the same patient in the ART application. Initiated for quality control of the ART plans, however, this study may offer some insights to more generalized applications in IMRT planning. Such generalization

should be applied with caution, and those factors affecting plan qualities should be considered when applying the tool to a new patent's IMRT plan.

V. CONCLUSIONS

An ART plan quality evaluation tool based on machine learning is developed. PCA and SVR are used to characterize and model the functional relationship between DVH and patient anatomical shape information. The DVH for a new treatment plan is estimated using its patient-specific anatomical information and an estimation model trained from high quality prior plans. The preliminary results show this tool's effectiveness in OAR sparing estimation and in providing evaluation guidance for ART approach.

ACKNOWLEDGMENTS

This work is partially supported by a master research grant from Varian Medical Systems.

[a]Author to whom correspondence should be addressed: Electronic mail: xiaofeng_zhu@med.unc.edu; Telephone: (919) 681-9627; Fax: (919) 681-7183.

[1]M. Ghilezan, D. Yan, and A. Martinez, "Adaptive radiation therapy for prostate cancer," Semin. Radiat. Oncol. **20**, 130–137 (2010).
[2]D. Yan, E. Ziaja, D. Jaffray, J. Wong, D. Brabbins, F. Vicini, and A. Martinez, "The use of adaptive radiation therapy to reduce setup error: A prospective clinical study," Int. J. Radiat. Oncol., Biol., Phys. **41**, 715–720 (1998).
[3]D. Yan, F. Vicini, J. Wong, and A. Martinez, "Adaptive radiation therapy," Phys. Med. Biol. **42**, 123–132 (1997).
[4]H. Rehbinder, C. Forsgren, and J. Lof, "Adaptive radiation therapy for compensation of errors in patient setup and treatment delivery," Med. Phys. **31**, 3363–3371 (2004).
[5]M. Birkner, D. Yan, M. Alber, J. Liang, and F. Nusslin, "Adapting inverse planning to patient and organ geometrical variation: Algorithm and implementation," Med. Phys. **30**, 2822–2831 (2003).
[6]A. Mestrovic, A. Nichol, B. G. Clark, and K. Otto, "Integration of on-line imaging, plan adaptation and radiation delivery: Proof of concept using digital tomosynthesis," Phys. Med. Biol. **54**, 3803–3819 (2009).
[7]R. Mohan, X. D. Zhang, H. Wang, Y. X. Kang, X. C. Wang, H. Liu, K. Ang, D. Kuban, and L. Dong, "Use of deformed intensity distributions for on-line modification of image-guided IMRT to account for interfractional anatomic changes," Int. J. Radiat. Oncol., Biol., Phys. **61**, 1258–1266 (2005).
[8]L. E. Court, L. Dong, A. K. Lee, R. Cheung, M. D. Bonnen, J. O'Daniel, H. Wang, R. Mohan, and D. Kuban, "An automatic CT-guided adaptive radiation therapy technique by online modification of multileaf collimator leaf positions for prostate cancer," Int. J. Radiat. Oncol., Biol., Phys. **62**, 154–163 (2005).
[9]Y. Feng, C. Castro-Pareja, R. Shekhar, and C. Yu, "Direct aperture deformation: An interfraction image guidance strategy," Med. Phys. **33**, 4490–4498 (2006).
[10]L. E. Court, R. B. Tishler, J. Petit, R. Cormack, and L. Chin, "Automatic online adaptive radiation therapy techniques for targets with significant shape change: A feasibility study," Phys. Med. Biol. **51**, 2493–2501 (2006).
[11]Q. J. Wu, D. Thongphiew, Z. Wang, B. Mathayomchan, V. Chankong, S. Yoo, W. R. Lee, and F. F. Yin, "On-line re-optimization of prostate IMRT plans for adaptive radiation therapy," Phys. Med. Biol. **53**, 673–691 (2008).
[12]D. Yan, "Developing quality assurance processes for image-guided adaptive radiation therapy," Int. J. Radiat. Oncol., Biol., Phys. **71**, S28–32 (2008).
[13]G. A. Ezzell, J. W. Burmeister, N. Dogan, T. J. LoSasso, J. G. Mechalakos, D. Mihailidis, A. Molineu, J. R. Palta, C. R. Ramsey, B. J. Salter, J. Shi, P. Xia, N. J. Yue, and Y. Xiao, "IMRT commissioning: Multiple institution planning and dosimetry comparisons, a report from AAPM Task Group 119," Med. Phys. **36**, 5359–5373 (2009).
[14]D. Thongphiew, Q. J. Wu, W. R. Lee, V. Chankong, S. Yoo, R. McMahon, and F. F. Yin, "Comparison of online IGRT techniques for prostate IMRT treatment: Adaptive vs repositioning correction," Med. Phys. **36**, 1651–1662 (2009).
[15]L. M. Chin, P. Kijewski, G. K. Svensson, J. T. Chaffey, M. B. Levene, and B. E. Bjarngard, "A computer-controlled radiation therapy machine for pelvic and para-aortic nodal areas," Int. J. Radiat. Oncol., Biol., Phys. **7**, 61–70 (1981).
[16]M. M. Austin-Seymour, G. T. Chen, J. R. Castro, W. M. Saunders, S. Pitluck, K. H. Woodruff, and M. Kessler, "Dose volume histogram analysis of liver radiation tolerance," Int. J. Radiat. Oncol., Biol., Phys. **12**, 31–35 (1986).
[17]M. A. Hunt, A. Jackson, A. Narayana, and N. Lee, "Geometric factors influencing dosimetric sparing of the parotid glands using IMRT," Int. J. Radiat. Oncol., Biol., Phys. **66**, 296–304 (2006).
[18]A. S. Reese, S. K. Das, C. Curie, and L. B. Marks, "Integral dose conservation in radiotherapy," Med. Phys. **36**, 734–740 (2009).
[19]B. Wu, F. Ricchetti, G. Sanguineti, M. Kazhdan, P. Simari, M. Chuang, R. Taylor, R. Jacques, and T. McNutt, "Patient geometry-driven information retrieval for IMRT treatment plan quality control," Med. Phys. **36**, 5497–5505 (2009).
[20]H. H. Zhang, R. R. Meyer, L. Shi, and W. D. D'Souza, "The minimum knowledge base for predicting organ-at-risk dose-volume levels and plan-related complications in IMRT planning," Phys. Med. Biol. **55**, 1935–1947 (2010).
[21]K. M. Langen and D. T. Jones, "Organ motion and its management," Int. J. Radiat. Oncol., Biol., Phys. **50**, 265–278 (2001).
[22]J. D. Bauer, A. Jackson, M. Skwarchuk, and M. Zelefsky, "Principal component, Varimax rotation and cost analysis of volume effects in rectal bleeding in patients treated with 3D-CRT for prostate cancer," Phys. Med. Biol. **51**, 5105–5123 (2006).
[23]C. Cortes and V. Vapnik, "Support-vector networks," Mach. Learn. **20**, 273–297 (1995).
[24]S. Chen, S. Zhou, F. F. Yin, L. B. Marks, and S. K. Das, "Investigation of the support vector machine algorithm to predict lung radiation-induced pneumonitis," Med. Phys. **34**, 3808–3814 (2007).
[25]A. J. Smola and B. Scholkopf, "A tutorial on support vector regression," Stat. Comput. **14**, 199–222 (2004).
[26]A. J. Smola and B. Scholkopf, "On a kernel-based method for pattern recognition, regression, approximation, and operator inversion," Algorithmica **22**, 211–231 (1998).
[27]H. Drucker, C. J. C. Burges, L. Kaufman, A. Smola and V. Vapnik, "Support vector regression machines," Adv. Neural Inf. Process. Syst. **9**, 155–161 (1997).
[28]L. Hamel, *Knowledge Discovery with Support Vector Machines* (Wiley, Hoboken, NJ, 2009).
[29]M. Sohn, M. Alber, and D. Yan, "Principal component analysis-based pattern analysis of dose-volume histograms and influence on rectal toxicity," Int. J. Radiat. Oncol., Biol., Phys. **69**, 230–239 (2007).